Characterization of the Reaction Products of Laser-Ablated Lanthanide Metal Atoms with Molecular Hydrogen. Infrared Spectra of LnH, LnH_2, LnH_3, and LnH_4 Molecules in Solid Argon

Stephen P. Willson and Lester Andrews*

Department of Chemistry, University of Virginia, Charlottesville, Virginia 22901

Received: August 25, 1999; In Final Form: November 17, 1999

Infrared spectra of representative LnH_{1-4} lanthanide hydride molecules are observed in solid argon following reactions of the laser-ablated metal atoms with H_2. The LnH_2 dihydride is the major product and a stable $(H_2)LnH_2$ complex is observed for Ce and Pr. In addition, bands are also assigned to bridging hydrogen motions of several $(LnH)_2$ dimers. Supplementary density functional calculations of the lanthanide hydride reaction products reproduce general features of the spectra. Spectra of isolated molecular EuH_2 and solid stoichiometric EuH_2 reveal close correspondence, lending support to the molecular assignment and, by extrapolation, providing benchmark infrared frequencies for other lanthanide hydride solids based on their respective molecular vibrational modes.

Introduction

In the ongoing pursuit of better semiconductor materials, enormous interest in the lanthanide hydrides has taken root and considerable effort has been expended to understand and devise superior semiconducting and magnetic materials that incorporate lanthanide hydrides.[1−6] Most of the experimental work in this area concentrates on the solid-phase bulk hydrides, with the exception of YbH and LuH, which have been characterized by matrix[7] and gas phase[8−14] electronic spectra. Although theoretical publications concentrate on the lanthanide monohydrides,[15−19] there is also a calculation for CeH_4.[20] It will be of interest to compare the Ce and Nd lanthanide hydride spectra with their Th and U actinide hydride counterparts[21,22] for the manifestation of relativistic effects.[23] In similar studies with Zr and Hf, relativistic effects are manifest in the infrared spectra of ZrH_2/HfH_2 and ZrH_4/HfH_4.[24,25]

The present work was undertaken to further elucidate the hydrogen chemistry of the lanthanide materials by filling gaps in the experimental data available for the small lanthanide hydride molecules. Specifically, the vibrational fundamentals of all the inserted lanthanide dihydrides except promethium, as well as those of six trihydrides, four tetrahydrides, and three monohydrides are reported here for the first time isolated in solid argon matrices, as well as five monohydride dimers, which give rise to bridging hydrogen modes.

Comparison of infrared spectra of matrix isolated EuH_2 with spectra of solid-phase EuH_2 reveals a strong correlation between vibrations in the solid[26] and in the isolated molecule. The sharp terminal hydrogen and deuterium vibrations of the solid correspond with the uncoupled H and D motions of the HEuD isotopic molecule. Because the europium oxidation state in stoichiometric EuH_2 is identical to that of the isolated dihydride molecule, a terminal hydrogen atom in the solid experiences a chemical environment similar to that of the uncoupled hydrogen atom in HEuD and thus has a coincident vibrational frequency. Broad infrared absorptions in the solid are more than 180 cm^{-1} lower than the sharp terminal hydrogen frequencies[26] and almost certainly due to bridged hydrogen atoms. Extrapolation of this result for europium and comparison with the other lanthanide hydrides provides a firm footing for identification of terminal and bridged molecular hydrogen modes in argon matrices and a solid connection between the solid-phase semiconductor studies and the small molecule experimental results provided in this investigation.

Experimental Section

Lanthanide metal atoms supplied by laser vaporization of metal targets (all but radioactive promethium) were reacted with molecular hydrogen in argon matrices using techniques described in previous publications.[27−30] Most experiments used 2% H_2/Ar, however concentrations ranged from 10% to 0.5% H_2, and samples were deposited at a rate of 4−5 mmol/h for 1−2 h onto a CsI window held at 6−7 or 10−11 K. Samples of D_2, mixed $H_2 + D_2$, and HD were also employed. Infrared spectra were recorded at 0.5 cm^{-1} resolution with a Nicolet 750, 550, or 60SXR spectrometer after deposition and after each annealing or photolysis cycle.

The metal targets, Ce (99.99%), Pr−Lu (Johnson-Matthey 99.9%), were ablated with the 1064 nm fundamental of a YAG laser, typically with 5−50 mJ pulses. For low laser power experiments, a 10% transmitting neutral density filter was placed in the laser beam. Following deposition, argon matrices were annealed to 18−20 K, then subjected either to UV photolysis using a 175 W mercury street lamp (Philips H39KB) without the globe (240−580 nm) or first to tungsten lamp (Sylvania 2518, FCS 24 V) photolysis followed by the mercury arc.

Results

Product peaks observed for each metal are reported in Tables 1−13 along with their annealing and photolysis behaviors. Spectra of samples with high H_2 concentration (>3%) also contain a broad band at 4260 (3062) cm^{-1} due to the induced infrared fundamental of H_2 (D_2) in solid argon.[31] All spectra

10.1021/jp993038a CCC: $19.00
Published on Web 02/04/2000

TABLE 1: Product Absorptions (cm^{-1}) Observed for Laser-Ablated Ce Atoms with H_2 in Solid Argon

H_2	D_2	HD[a]	ratio[b]	anneal.[c]	ident.
1500.5	1070.2	1493.6, 1065.6	1.4021	a++(−)	CeH_4 s str
1486.3	1059.8		1.4024	b+	CeH_2^+ ν_1
1459.3	1044.7	1477.9, 1055.9	1.3969	b+	?
1445.9	1035.3	1466.2, 1047.5	1.3966	b+(−)	CeH_2^+ ν_3
1441.8	1032.1	1449.4, 1036.2	1.3970	a++(−)	CeH_4 a str
1388.2	1019.8	1388.2, 1019.8	1.3612	a++	HO_2
1330.7	943.7		1.4101	a0−(+ −)	CeH_2 ν_1
1298.8	927.5		1.4003	b+(−)	$(H_2)CeH_2$ s str
1283.1	918.0	1281.6, 918.6	1.3977	a+ −	CeH_3
1281.7	916.9	1306.4, 932.3	1.3979	a0−(+ −)	CeH_2 ν_3
1271	910.5	1271, 910.6	1.396	a+ −	(CeH)
1248.6	894.2	1273.3, 910.3	1.3963	b+(−)	$(H_2)CeH_2$ a str
		1248.0, 895.1	1.3943	b+	$(H_2)CeH_2$ a str
		1195.8, 843.3	1.4180	a+ −	$(CeH)_2$ s str
1128.0	808.3	1125.4, 809.5	1.3955	a+ −	$(CeH)_2$ a str
903.2	643.1		1.4044	a+ −(−)	Ar_nH^+

[a] HD counterparts of the LnH_2 molecules are listed in the same row as the antisymmetric stretch of the pure isotopic species, although this designation does not apply for the HLnD molecule. [b] Ratio of H_2/D_2 isotopic frequencies. [c] Annealing behavior: a denotes presence on deposition, +, −, or 0 indicates the direction of growth in two successive annealings, b denotes appearance on the first annealing and +, −, or 0 indicates changes on second annealing, (+ or −) indicates changes on photolysis, (+ −) indicates an increase with tungsten lamp photolysis and a decrease with Hg arc photolysis.

TABLE 2: Product Absorptions (cm^{-1}) Observed for Laser-Ablated Pr Atoms with H_2 in Solid Argon

H_2	D_2	HD[a]	ratio[b]	anneal.[c]	ident.
1296.8	924.0	- - -, - - -	1.4035	a− −	?
1286.6	917.2	- - -, - - -	1.4027	a0(+-)	PrH_2
1248.1	894.1	1264.0, - - -	1.3961	a++(−)	$(H_2)PrH_2$
		1207.1, 852.2	1.4165	a+ −(+)	$(PrH)_2$ s str
1135.6	813.4	1133.2, 817.2	1.3961	a+ −(+)	$(PrH)_2$ a str

[a] HD counterparts of the LnH_2 molecules are listed in the same row as the antisymmetric stretch of the pure isotopic species, although this designation does not apply for the HLnD molecule. [b] Ratio of H_2/D_2 isotopic frequencies. [c] Annealing behavior: a denotes presence on deposition, +, −, or 0 indicates the direction of growth in two successive annealings, b denotes appearance on the first annealing and +, −, or 0 indicates changes on second annealing, (+ or −) indicates changes on photolysis, (+ −) indicates an increase with tungsten lamp photolysis and a decrease with Hg arc photolysis.

contained very weak LnO and LnO_2 absorptions, presumably from surface oxide ablation, since there was no sign of molecular oxygen complexes or ozone.[32,33] Representative spectra are provided in Figures 1−6.

Calculations

Theoretical calculations were performed for several lanthanide hydride species with the Amsterdam density functional (ADF 2.1) program developed by Baerends et al.[34−36] Exchange and correlation were accounted for using the Vosko, Wilk, and Nusair parametrized local density approximation,[37] and nonlocal exchange and correlation corrections were handled by the Becke and Perdew method (BP86).[38,39] The numerical integration parameter was set to 6.0, which is expected to provide reasonably accurate geometries and vibrational frequencies.[36] The basis sets were triple-ζ with one polarization function included for the H atoms, but without polarization functions for the Ln metal atoms (ADF 2.1, Basis Set IV). The Ln atoms were frozen through the 4d level. First-order relativistic scalar corrections and diagonalization in the nonrelativistic basis yielded quasi-relativistic solutions.[40] Computational results are provided in Table 14.

TABLE 3: Product Absorptions (cm^{-1}) Observed for Laser-Ablated Nd Atoms with H_2 in Solid Argon

H_2	D_2	HD[a]	ratiob	anneal.[c]	ident.
1384.6	986.3	1359.4, 967.0, 1331.2, 950.6	1.4038	a+ −	NdH_4 s str
1304.3, 1300.7	935.5, 931.6	1301.7, 935.0	1.3942, 1.3962	a+ −	NdH_4 a str
1196.7	855.2	1196.7, 855.2	1.3993	a++	NdH
1194.2	852.9	1194.2, 852.9	1.4002	a++	NdH site
1177.5	841.3		1.3996	a0−	NdH site
1150.0	824.6	1148.7, 826.8	1.3946	a++(+)	NdH_3 a str
1148.4	822.4	1170.4, 836.7	1.3964	a+ −	NdH_2 ν_3
		1218.3, 860.6	1.4156	a++(+)	NdH_2D (NdD_2H)

[a] HD counterparts of the LnH_2 molecules are listed in the same row as the antisymmetric stretch of the pure isotopic species, although this designation does not apply for the HLnD molecule. [b] Ratio of H_2/D_2 isotopic frequencies. [c] Annealing behavior: a denotes presence on deposition, +, −, or 0 indicates the direction of growth in two successive annealings, b denotes appearance on the first annealing and +, −, or 0 indicates changes on second annealing, (+ or −) indicates changes on photolysis, (+ −) indicates an increase with tungsten lamp photolysis and a decrease with Hg arc photolysis.

TABLE 4: Product Absorptions (cm^{-1}) Observed for Laser-Ablated Sm Atoms with H_2 in Solid Argon

H_2	D_2	HD[a]	ratio[b]	anneal.[c]	ident.
1331.4, 1328.7	954.1, 952.1	1328.9, 953.9	1.3955	a− −(+)	SmH_4
1213.0	864.3		1.4034	a− −(+)	SmH_2 ν_1
1203.5	857.0	1202.5, 860.2	1.4043	a0−	SmH_3 a str
		1184.1, 844.6	1.4020	a− −(+)	SmHD
1156.5	827.2		1.3981	a− −(+)	SmH_2 ν_3

[a] HD counterparts of the LnH_2 molecules are listed in the same row as the antisymmetric stretch of the pure isotopic species, although this designation does not apply for the HLnD molecule. [b] Ratio of H_2/D_2 isotopic frequencies. [c] Annealing behavior: a denotes presence on deposition, +, −, or 0 indicates the direction of growth in two successive annealings, b denotes appearance on the first annealing and +, −, or 0 indicates changes on second annealing, (+ or −) indicates changes on photolysis, (+ −) indicates an increase with tungsten lamp photolysis and a decrease with Hg arc photolysis.

TABLE 5: Product Absorptions (cm^{-1}) Observed for Laser-Ablated Eu Atoms with H_2 in Solid Argon

H_2	D_2	HD[a]	ratio[b]	anneal.[c]	ident.
1211.7	863.6		1.4031	a0−(+)	EuH_2 ν_1
		1156.9, 827.8	1.3976	a+0	(EuH_2D) (EuD_2H)
1155.6	827.0	1183.5, 844.1	1.3973	a0−(+)	EuH_2 ν_3

[a] HD counterparts of the LnH_2 molecules are listed in the same row as the antisymmetric stretch of the pure isotopic species, although this designation does not apply for the HLnD molecule. [b] Ratio of H_2/D_2 isotopic frequencies. [c] Annealing behavior: a denotes presence on deposition, +, −, or 0 indicates the direction of growth in two successive annealings, b denotes appearance on the first annealing and +, −, or 0 indicates changes on second annealing, (+ or −) indicates changes on photolysis, (+ −) indicates an increase with tungsten lamp photolysis and a decrease with Hg arc photolysis.

Discussion

The lanthanide metal−hydrogen systems all contain similar products of reaction, which are identified as LnH, LnH_2, LnH_3, LnH_4, and $(LnH)_2$ species. Since all of the molecular isotopic variations are observed in either the pure isotopic or in the HD samples, and H_2/D_2 spectra provide overlapping isotopic peaks; the H_2/D_2 absorptions are not listed in Tables 1−13, but are referred to in the discussion to complement the assignments. Lanthanide hydride frequencies are used in the text with lanthanide deuteride absorptions supplied parenthetically.

TABLE 6: Product Absorptions (cm^{-1}) Observed for Laser-Ablated Gd Atoms with H_2 in Solid Argon

H_2	D_2	HD[a]	ratio[b]	anneal.[c]	ident.
1521.1	1088.5		1.3974	a+ −	GdH_2^+ ν_3 ?
1445.2	1033.1		1.3989	a+0	?
1426.9	1018.6		1.4008	a− −(+)	GdH_2 ν_1 site
1404.0	1002.0		1.4012	a− −(+)	GdH_2 ν_1 site
1399.0	998.8		1.4007	a+ −(+)	GdH_2 ν_1
1379.3	987.2	1402.3, 1001.5	1.3972	a− −(+)	GdH_2 ν_3 site
1364.4	976.8	1383.1, 988.0	1.3968	a− −(+)	GdH_2 ν_3 site
1359.3	973.0	1379.8, 985.4	1.3970	a+ −(+)	GdH_2 ν_3
		1357.7, 974.1	1.3938	a++	GdH_3 a str site
1346.1	963.7	1345.7, 962.7	1.3968	a++	?
1323.6	947.5	1323.1, 948.9	1.3969	a++	GdH_3 a str
		1264.5, 894.9	1.4130	a++(+)	$(GdH)_2$ s str
1201.9	860.9	1199.7, 863.3	1.3961	a++(+)	$(GdH)_2$ a str

[a] HD counterparts of the LnH_2 molecules are listed in the same row as the antisymmetric stretch of the pure isotopic species, although this designation does not apply for the HLnD molecule. [b] Ratio of H_2/D_2 isotopic frequencies. [c] Annealing behavior: a denotes presence on deposition, +, −, or 0 indicates the direction of growth in two successive annealings, b denotes appearance on the first annealing and +, −, or 0 indicates changes on second annealing, (+ or −) indicates changes on photolysis, (+ −) indicates an increase with tungsten lamp photolysis and a decrease with Hg arc photolysis.

TABLE 7: Product Absorptions (cm^{-1}) Observed for Laser-Ablated Tb Atoms with H_2 in Solid Argon

H_2	D_2	HD[a]	ratio[b]	anneal.[c]	ident.
1539.3	1101.8		1.3971	a− −(+)	TbH_2^+ ν_3 ?
1480.0	1057.8	1480.1, 1057.6	1.3991	a+ −	TbH site
1469.1	1050.1	1469.1, 1050.1	1.3990	a+ −	TbH
1445.3	1031.4		1.4013	a− −(+)	TbH_2 ν_1
1428.9	1019.8		1.4012	a− −(+)	TbH_2 ν_1 site
1391.1	996.0	1418.5, 1013.4	1.3967	a− −(+)	TbH_2 ν_3
1376.7	986.1	1402.6, 1002.0	1.3961	a− −(+)	TbH_2 ν_3 site
1375.5	985.2	1374.3, 986.7	1.3962	a− −(+)	TbH_3
1349.5	966.3	1349.0, 966.5	1.3966	a++	TbH_3 site
1212.1	868.8	1209.9, 871.1	1.3951	a+ −	$(TbH)_2$ a str
1159.9	832.3	1160.3, 835.1	1.3936	b+	$(TbH_2)_2$ a str

[a] HD counterparts of the LnH_2 molecules are listed in the same row as the antisymmetric stretch of the pure isotopic species, although this designation does not apply for the HLnD molecule. [b] Ratio of H_2/D_2 isotopic frequencies. [c] Annealing behavior: a denotes presence on deposition, +, −, or 0 indicates the direction of growth in two successive annealings, b denotes appearance on the first annealing and +, −, or 0 indicates changes on second annealing, (+ or −) indicates changes on photolysis, (+ −) indicates an increase with tungsten lamp photolysis and a decrease with Hg arc photolysis.

TABLE 8: Product Absorptions (cm^{-1}) Observed for Laser-Ablated Dy Atoms with H_2 in Solid Argon

H_2	D_2	HD[a]	ratio[b]	anneal.[c]	ident.
		1409.8, 1009.2	1.3969	a+ −(+)	DyH_4 s str
1386.5	992.9	1385.0, 994.8	1.3964	a+ −(+)	DyH_4 a str
1247.1	888.6		1.4034	a0−(+-)	DyH_2 ν_1
1193.1	853.8	1219.3, 870.4	1.3974	a0−(+-)	DyH_2 ν_3

[a] HD counterparts of the LnH_2 molecules are listed in the same row as the antisymmetric stretch of the pure isotopic species, although this designation does not apply for the HLnD molecule. [b] Ratio of H_2/D_2 isotopic frequencies. [c] Annealing behavior: a denotes presence on deposition, +, −, or 0 indicates the direction of growth in two successive annealings, b denotes appearance on the first annealing and +, −, or 0 indicates changes on second annealing, (+ or −) indicates changes on photolysis, (+ −) indicates an increase with tungsten lamp photolysis and a decrease with Hg arc photolysis.

Because all of the metal hydride frequencies observed have an H/D isotopic frequency ratio very close to 1.4, the identifications are more dependent upon the isotopic peak shifting behavior and relative positions of hydride stretches than on the hydrogen isotopic ratios. Nonetheless, the ratios do provide some guidance, as symmetric stretches generally have ratios greater than 1.4 and are weaker, and antisymmetric motions have ratios less than 1.4 and are relatively stronger. The isotopic patterns

TABLE 9: Product Absorptions (cm^{-1}) Observed for Laser-Ablated Ho Atoms with H_2 in Solid Argon

H_2	D_2	HD[a]	ratio[b]	anneal.[c]	ident.
1339	960	1364, 976	1.395	b+	aggregate
1255.8	895.1		1.4030	a+ −(+)	HoH_2 ν_1
1203.6	861.3	1229.5, 877.4	1.3974	a+ −(+)	HoH_2 ν_3

[a] HD counterparts of the LnH_2 molecules are listed in the same row as the antisymmetric stretch of the pure isotopic species, although this designation does not apply for the HLnD molecule. [b] Ratio of H_2/D_2 isotopic frequencies. [c] Annealing behavior: a denotes presence on deposition, +, −, or 0 indicates the direction of growth in two successive annealings, b denotes appearance on the first annealing and +, −, or 0 indicates changes on second annealing, (+ or −) indicates changes on photolysis, (+ −) indicates an increase with tungsten lamp photolysis and a decrease with Hg arc photolysis.

TABLE 10: Product Absorptions (cm^{-1}) Observed for Laser-Ablated Er Atoms with H_2 in Solid Argon

H_2	D_2	HD[a]	ratio[b]	anneal.[c]	ident.
1418.6	1019.7		1.3912	a0−(+)	Er_xH_y
1410.6	1010.2	1442.3, 1029.7	1.3964	a0−(+)	Er_xH_y
1271.0	905.7		1.4033	a0−(+)	ErH_2 ν_1
1217.3	871.3	1244.1, 888.1	1.3971	a0−(+)	ErH_2 ν_3

[a] HD counterparts of the LnH_2 molecules are listed in the same row as the antisymmetric stretch of the pure isotopic species, although this designation does not apply for the HLnD molecule. [b] Ratio of H_2/D_2 isotopic frequencies. [c] Annealing behavior: a denotes presence on deposition, +, −, or 0 indicates the direction of growth in two successive annealings, b denotes appearance on the first annealing and +, −, or 0 indicates changes on second annealing, (+ or −) indicates changes on photolysis, (+ −) indicates an increase with tungsten lamp photolysis and a decrease with Hg arc photolysis.

TABLE 11: Product Absorptions (cm^{-1}) Observed for Laser-Ablated Tm Atoms with H_2 in Solid Argon

H_2	D_2	HD[a]	ratio[b]	anneal.[c]	ident.
1370	982	1394, 998	1.395	b+	Tm_xH_y
1281.2	913.3		1.4028	a++(+ −)	TmH_2 ν_1
1222.2	874.8	1251.6, 893.0	1.3971	a++(+ −)	TmH_2 ν_3

[a] HD counterparts of the LnH_2 molecules are listed in the same row as the antisymmetric stretch of the pure isotopic species, although this designation does not apply for the HLnD molecule. [b] Ratio of H_2/D_2 isotopic frequencies. [c] Annealing behavior: a denotes presence on deposition, +, −, or 0 indicates the direction of growth in two successive annealings, b denotes appearance on the first annealing and +, −, or 0 indicates changes on second annealing, (+ or −) indicates changes on photolysis, (+ −) indicates an increase with tungsten lamp photolysis and a decrease with Hg arc photolysis.

TABLE 12: Product Absorptions (cm^{-1}) Observed for Laser-Ablated Yb Atoms with H_2 in Solid Argon

H_2	D_2	HD[a]	ratio[b]	anneal.[c]	ident.
1276.1	910.0		1.4023	a+ −(+)	YbH_2 ν_1
1218.6	872.1	1247.8, 890.0	1.3973	a+ −(+)	YbH_2 ν_3

[a] HD counterparts of the LnH_2 molecules are listed in the same row as the antisymmetric stretch of the pure isotopic species, although this designation does not apply for the HLnD molecule. [b] Ratio of H_2/D_2 isotopic frequencies. [c] Annealing behavior: a denotes presence on deposition, +, −, or 0 indicates the direction of growth in two successive annealings, b denotes appearance on the first annealing and +, −, or 0 indicates changes on second annealing, (+ or −) indicates changes on photolysis, (+ −) indicates an increase with tungsten lamp photolysis and a decrease with Hg arc photolysis.

TABLE 13: Product Absorptions (cm^{-1}) Observed for Laser-Ablated Lu Atoms with H_2 in Solid Argon

H_2	D_2	HD[a]	ratio[b]	anneal.[c]	ident.
1486.4	1061.3		1.4005	a− −(−)	LuH_2 ν_1
1445.0	1030.8	1443.6, 1035.9	1.4018	a0−(+)	?
1426.4	1021.5	1456.7, 1040.5	1.3964	a− −(−)	LuH_2 ν_3
		1410.6, 1009.7	1.3970	b+	?
1386.4	993.9	1385.6, 994.5	1.3949	a++(−)	LuH_3 a str
		1332.9, 944.5	1.4112	a+ −(+)	$(LuH)_2$ s str
1273.2	912.1	1271.3, 914.4	1.3959	a+ −(+)	$(LuH)_2$ a str

[a] HD counterparts of the LnH_2 molecules are listed in the same row as the antisymmetric stretch of the pure isotopic species, although this designation does not apply for the HLnD molecule. [b] Ratio of H_2/D_2 isotopic frequencies. [c] Annealing behavior: a denotes presence on deposition, +, −, or 0 indicates the direction of growth in two successive annealings, b denotes appearance on the first annealing and +, −, or 0 indicates changes on second annealing, (+ or −) indicates changes on photolysis, (+ −) indicates an increase with tungsten lamp photolysis and a decrease with Hg arc photolysis.

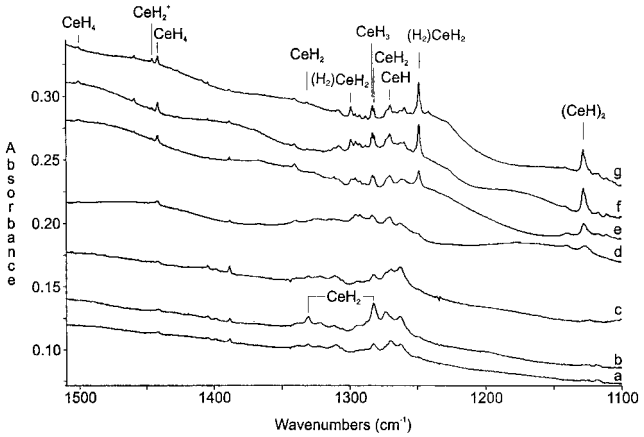

Figure 1. Infrared spectra in the 1510−1100 cm^{-1} region for laser-ablated cerium atoms codeposited with 2% H_2:Ar after (a) 1 h deposition with low laser power, (b) 15 min tungsten lamp photolysis, (c) 15 min Hg arc photolysis, (d) 1 h deposition with high laser power, (e) 20 K annealing, (d) 25 K annealing, and (e) 30 K annealing.

for each molecule type are detailed preceding each section and referred to in individual characterizations for each species.

Low laser power experiments, which use $^1/_{10}$th of the laser power of high-power experiments, produce fewer products containing an odd number of H atoms than do high-power counterparts and are completely lacking in dimetal species. The most intense product absorption in these spectra is the ν_3 (b_1) fundamental of the monometal dihydride (LnH_2, C_{2v}), with weak tetrahydride absorptions also present. The decline in LnH and LnH_3 intensities is attributed to the weaker laser plume, which atomizes molecular H_2 less effectively. Dimetal species are disfavored as a consequence of the substantial reduction in metal concentration brought about by an order of magnitude decrease in laser power.

Solid-phase infrared spectra of EuH_2 provide a sharp peak at 1180 cm^{-1} and broad peaks at 994, 959, 830, and 620 cm^{-1}.[26] The sharp peak is here attributed to terminal hydrogen atoms in the solid owing to coincidence with the uncoupled HEuD molecular vibration; the broad peaks involve bridging hydrogen motions, supporting assignment of peaks in lanthanide hydride molecular spectra about 150 cm^{-1} lower than the molecular dihydrides to bridging hydrogen stretches.

Density functional calculations of lanthanide hydride molecules (Table 14) provide broad support for the experimental assignments. Most calculated frequencies are within 50 cm^{-1} (4%) of the observed values, CeH_4 being a notable exception.

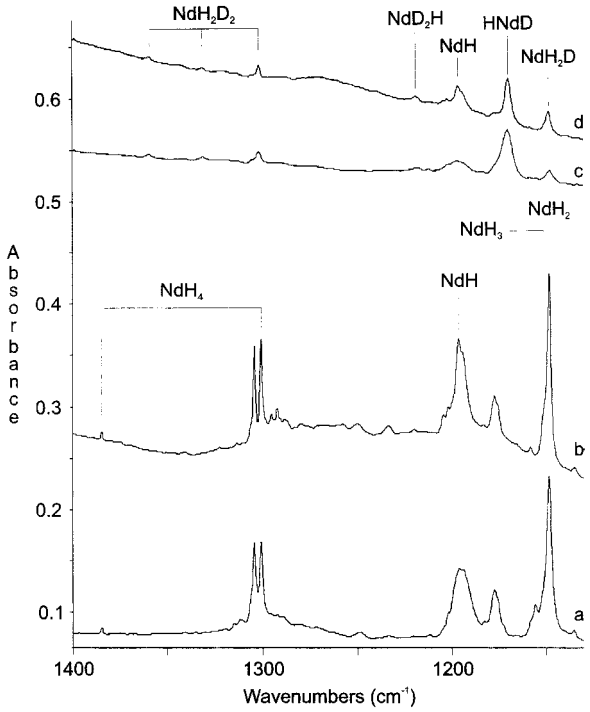

Figure 2. Infrared spectra in the 1400−1130 cm^{-1} region for laser-ablated neodymium atoms codeposited with (a) 2% H_2:Ar after 1 h deposition, (b) 2% H_2:Ar after 30 K annealing, (c) 2% HD:Ar after 1 h deposition, and (d) 2% HD:Ar after 27 K annealing.

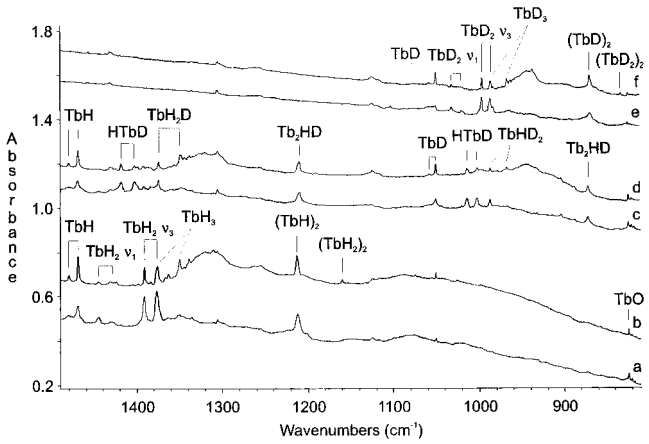

Figure 3. Infrared spectra in the 1490−810 cm^{-1} region for laser-ablated terbium atoms codeposited with (a) 2% H_2:Ar after 2.5 h deposition, (b) 2% H_2:Ar after 30 K annealing, (c) 3% HD:Ar after 2.5 h deposition, (d) 3% HD:Ar after 30 K annealing, (e) 2% D_2:Ar after 2 h deposition, and (f) 2% D_2:Ar after 30 K annealing.

The calculated frequencies of the LnH_2 ν_3 (b_1) modes and the LnH_3 ν_3 (e) modes are very close to each other for Ce, Gd, and Tb, which is consistent with the near coincidence of these two vibrations observed for several lanthanide hydride systems.

LnH Species. Three lanthanide monohydride vibrations are observed in spectra of the reaction products of lanthanide metal atom reactions with molecular H_2. Because the metal hydride products cannot be easily distinguished by hydrogen isotopic ratios, the monohydrides are classified by the lack of isotopic shift in HD experiments, which is a unique property of the monohydrides. The experimentally observed fundamentals are in accord with density functional and pseudopotential calculations for these modes.[17]

A broad absorption at 1271 (910.5) cm^{-1} (Table 1) that increases with annealings up to 25 K (Figure 1) and does not

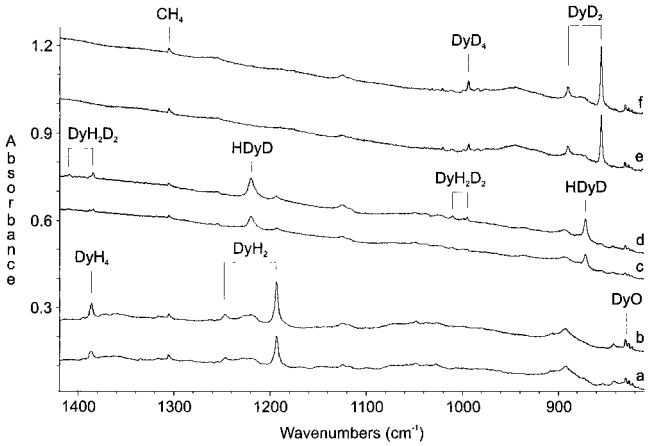

Figure 4. Infrared spectra in the 1420−810 cm^{-1} region for laser-ablated dysprosium atoms codeposited with (a) 2% H_2:Ar after 2 h deposition, (b) 2% H_2:Ar after 0.5 h Hg arc photolysis, (c) 3% HD:Ar after 2 h deposition, (d) 3% HD:Ar after 0.5 h Hg arc photolysis, (e) 2% D_2:Ar after 2 h deposition, and (f) 2% D_2:Ar after 0.5 h Hg arc photolysis.

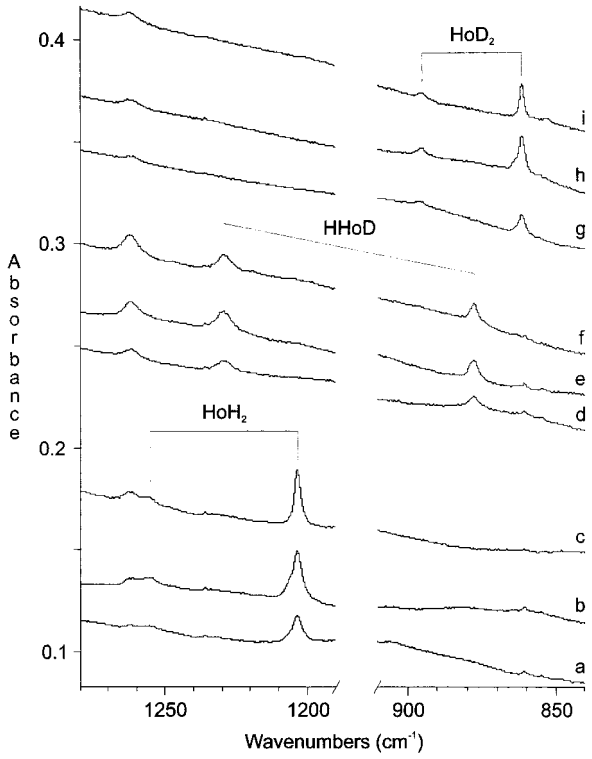

Figure 5. Infrared spectra in the 1280−1190 and 910−840 cm^{-1} regions for laser-ablated holmium atoms codeposited with (a) 2% H_2:Ar after 45 min deposition, (b) 2% H_2:Ar after 15 min tungsten lamp photolysis, (c) 2% H_2:Ar after 25 K annealing, (d) 3% HD:Ar after 1 h deposition, (e) 3% HD:Ar after 18 min tungsten lamp photolysis, (f) 3% HD:Ar after 25 K annealing, (g) 2% D_2:Ar after 1 h deposition, (h) 2% D_2:Ar after 13 min tungsten lamp photolysis, and (i) 2% D_2:Ar after 25 K annealing.

measurably shift upon HD isotopic substitution is tentatively assigned to CeH. This assignment is supported by density functional calculations, which predict 1312 cm^{-1} for the harmonic CeH vibrational fundamental.

Neodymium monohydride absorbs at 1196.7 (855.2) cm^{-1} (Table 3 and Figure 2) with a significant matrix splitting at 1177.5 (841.3) cm^{-1}. The H/D isotopic ratio of 1.3993 is indicative of a hydrogen stretching motion and the peak is favored by low H_2 concentrations and in microwave discharge experiments. This suggests that the absorber contains a low

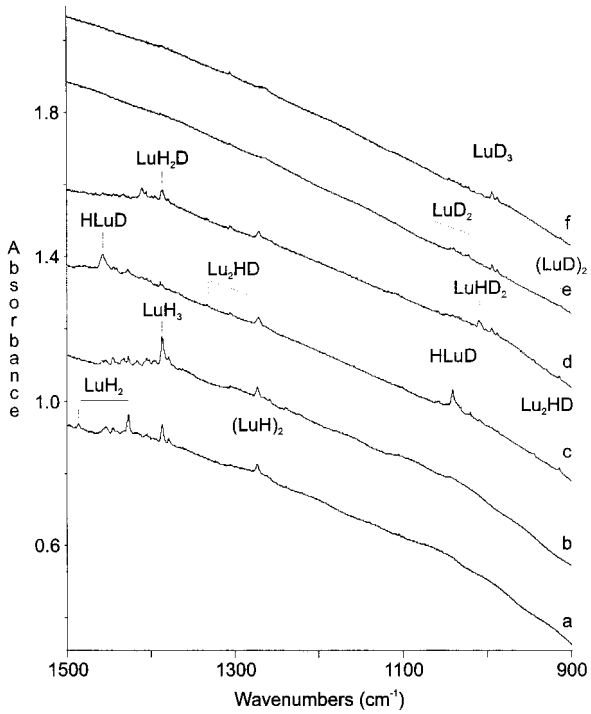

Figure 6. Infrared spectra in the 1500−900 cm^{-1} region for laser-ablated lutetium atoms codeposited with (a) 2% H_2:Ar after 1 h 20 min deposition, (b) 2% H_2:Ar after 35 K annealing, (c) 3% HD:Ar after 1 h deposition, (d) 3% HD:Ar after 35 K annealing, (e) 2% D_2:Ar after 1 h deposition, and (f) 2% D_2:Ar after 35 K annealing.

hydrogen content relative to the other metal hydride species and likely has an odd number of hydrogen atoms, because it is favored under discharge conditions, which provide higher concentrations of atomic hydrogen relative to samples that have not been discharged. The calculated pseudopotential frequency[17] of 1133 cm^{-1} for the corresponding state of NdH may be compared with this experimental observation.

A strong sharp absorption at 1469.1 (1050.1) cm^{-1} with a weaker site at 1480.0 (1057.8) cm^{-1} (Table 7 and Figure 3) is assigned to the stretching fundamental of isolated terbium monohydride. The position of this band is invariant in isotopically substituted HD experiments and no other peaks track with it through photolysis and annealing, which strongly indicates a monohydride species. This assignment is in accord with the calculated density functional value of 1429 cm^{-1} and the earlier pseudopotential value[17] of 1409 cm^{-1} for the TbH vibrational fundamental.

LnH_2 Species. In the solid phase, all of the lanthanide metals react directly with molecular H_2 to form the nonstoichiometric dihydride.[41] The molecular lanthanide dihydride insertion product is the most prevalent species observed in spectra of ablated lanthanide atoms deposited with molecular hydrogen into argon matrices. Bent LnH_2 molecules (C_{2v}) have been identified for all of the lanthanides except promethium and are discussed in the ensuing sections and assigned in the tables. The characteristic LnH_2 molecule infrared spectrum displays both the ν_1 (a_1) and ν_3 (b_1) fundamentals for the LnH_2 and LnD_2 molecules; the ν_1 (a_1) mode exhibits a slightly higher H/D ratio than the ν_3 (b_1) mode, as expected for normal modes of different symmetry.[42] When isotopically substituted HD is employed, two modes are observed for the HLnD molecules, one that occurs within 0.5 cm^{-1} of the average of the LnH_2 ν_1 and ν_3 fundamentals and a second that occurs within 2.0 cm^{-1} of the average of the LnD_2 ν_1 and ν_3 fundamentals. This isotopic pattern is unique to the dihydrides, which also have a

TABLE 14: Results of Density Functional Calculations for Select Lanthanide Hydrides

molecule	multipl	bond length (Å)	angle (deg)	calcd freq (cm^{-1})	intensity (km/mol)	exptl freq (cm^{-1})
CeH	quartet	2.08		1311.8	440	1271
CeH_2	triplet	2.08	109.6	431.7 (a_1)	140	1281.7
				1332.6 (b_1)	700	1330.7
				1341.9 (a_1)	550	
$(H_2)CeH_2$	triplet	Ce−H 2.10	113.8	486.5 (a_1)	170	1298.8
		H−H 0.84		1280.8 (a_1)	520	1248.6
				1286.5 (b_2)	970	
				2883.8 (a_1)	830	
CeH_2^+	doublet	1.98	114.9	525.6 (a_1)	90	
				1493.8 (b_1)	500	1445.9
				1544.1 (a_1)	160	1486.3
CeH_3	doublet	2.07	108.5	320.4 (a_1)	350	
				480.2 (e)	100	
				1326.9 (e)	970	1283.1
				1399.0 (a_1)	220	
CeH_4	singlet	2.01	109.5	413.8 (t_2)	270	
				555.6 (e)	0	
				1359.6 (t_2)	730	1441.8
				1390.4 (a_1)	0	1500.5
$(CeH)_2$	triplet	Ce−Ce 2.54		188.7 (a_{1g})	0	
		Ce−H 2.15		219.8 (b_{1u})	10	
				952.8 (b_{1g})	0	
				974.5 (b_{3u})	170	
				1117.2 (b_{2u})	200	1128.0
				1155.2 (a_{1g})	0	
PrH_2	quartet	2.06	109.3	460.0 (a_1)	110	
				1277.6 (b_1)	650	1248.1
				1283.9 (a_1)	680	
SmH_2	quintet	2.05	107.2	278.7 (a_1)	90	
				1162.7 (b_1)	80	1156.5
				1179.1 (a_1)	40	1213.0
SmH_3	sextet	2.06	108.3	45.4 (e)	340	
				326.3 (a_1)	320	
				1182.4 (e)	300	1203.5
				1226.7 (a_1)	80	
EuH_2	octet	2.08	109.6	462.6 (a_1)	60	
				1226.1 (b_1)	680	1155.6
				1240.7 (a_1)	440	1211.7
EuH_3	heptet	2.05	109.1	353.5 (a_1)	370	
				551.7 (e)	3	
				1140.5 (e)	70	(1156.9)
				1255.2 (a_1)	80	
GdH_2	nonet	1.98	111.7	435.9 (a_1)	130	
				1402.6 (b_1)	640	1359.3
				1446.3 (a_1)	210	1399.0
GdH_3	octet	1.99	108.9	306.1 (a_1)	370	
				523.0 (e)	60	
				1399.8 (e)	760	1323.6
				1456.9 (a_1)	80	
TbH	heptet	1.97		1429.4	310	1469.1
TbH_2	octet	2.01	114.9	419.0 (a_1)	130	
				1354.1 (b_1)	700	1391.1
				1407.3 (a_1)	210	1445.3
TbH_3	heptet	2.02	108.3	287.3 (a_1)	440	
				519.1 (e)	130	
				1354.0 (e)	1600	1375.5
				1417.3 (a_1)	50	

tendency to increase with tungsten lamp photolysis and decrease with successive Hg arc photolysis. The LnH_2 species are primarily formed by direct insertion of an ablated Ln atom into the molecular hydrogen bond and generally only bands due to the HLnD isotopically substituted species are present in HD samples.

The average Ln−H stretching frequencies of the LnH_2 species are plotted (Figure 7); two lines about 170 cm^{-1} apart are found, the higher with a slope of 11.7 cm^{-1} and the lower with a slope of 9.0 cm^{-1}. As a difference in frequency of about 150 cm^{-1} characterizes two primary electronic structures found for the lanthanide monoxide species,[33,43] the difference of about 170 cm^{-1} found for the lanthanide dihydrides is also taken to indicate the prevalence of two basic electronic structures within the dihydride series, which are suggested to be $f^{n-1}s$ for the upper and f^n for the lower line; PrH_2 is not plotted, as this assignment

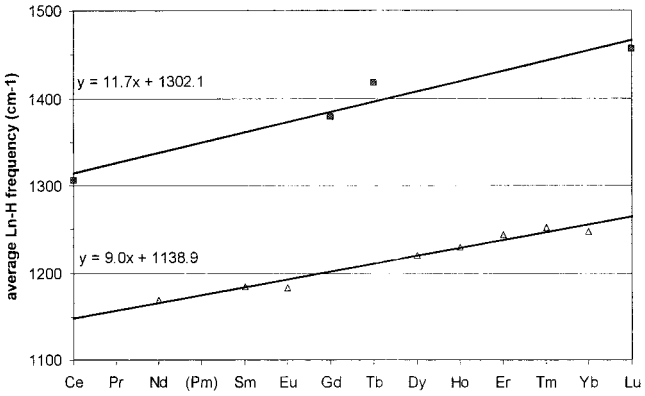

Figure 7. Plot of the average Ln-H stretching frequencies for the LnH_2 molecules.

is tentative. In addition, BaH_2 and LaH_2 have been observed in this laboratory (unpublished) at 1068 and 1283 cm^{-1}. These molecules fall just below the extended lower and upper lines, respectively, where the two differ by the presence of a nonbonded 6s electron.

A strong absorption at 1281.7 (916.9) cm^{-1} in spectra of atomic Ce and molecular H_2 deposited into argon and a weaker complementary peak at 1330.7 (943.7) cm^{-1} are assigned, respectively, to the ν_3 and ν_1 fundamentals of the inserted CeH_2 dihydride (Table 1 and Figure 1). In high laser power experiments, the ν_3 band overlaps with a second band of comparable intensity following deposition but is separated from the second peak following 22 K annealing, which intensifies and sharpens both bands. Neither band in the high power experiments is affected by Hg arc photolysis, and both decline after annealings higher than 25 K. In low laser power experiments, CeH_2 is the dominant product and triples with tungsten lamp photolysis but declines with subsequent Hg arc photolysis back to its original intensity. This suggests that visible photolysis excites Ce, as this region is rich in strong electronic transitons,[44] and activates direct insertion into H_2, reaction 1, but UV irradiation photo-

$$Ce + H_2 \rightarrow CeH_2 \quad (1)$$

dissociates the CeH_2 molecule. Spectra of Ce reacted with isotopically substituted HD provide HCeD fundamentals at 1306.4 and 932.3 cm^{-1}, only 0.2 (2.0) cm^{-1} away from the average of the ν_1 and ν_3 fundamentals of the isotopically pure molecules, which confirms the MH_2 vibrational mechanics and metal dihydride identification.

Bands at 1486.3 (1059.8) and 1445.9 (1035.3) cm^{-1} that appear after annealing and increase up to 30 K are respectively assigned to the ν_1 (a_1) and ν_3 (b_1) fundamentals of the CeH_2^+ cation. These bands demonstrate CeH_2 isotopic behavior, with a hydrogen isotopic ν_1 ratio higher than the ν_3 ratio and $HCeD^+$ absorptions at 1466.2 and 1047.5 cm^{-1}, 0.1 cm^{-1} away from the ν_1 and ν_3 averages for the isotopically pure products. In spectra of samples using low laser power to ablate the cerium target, the dihydride cation is not present. Cerium dihydride cation is formed in reaction 2 by insertion of Ce^+, from laser ablation, into dihydrogen.

$$Ce^+ + H_2 \rightarrow CeH_2^+ \quad (2)$$

The CeH_2 and CeH_2^+ assignments are supported by the ADF calculations (Table 14). For the strongest ν_3 (b_1) modes the scale factors (observed/calculated) are 0.962 and 0.968, respectively, which are appropriate for this calculation. Note that the calculation predicts a 161 cm^{-1} blue shift for CeH_2^+ relative to CeH_2 and 162 cm^{-1} is observed. The ν_3 (b_1) fundamentals of

the 12 remaining lanthanide dihydrides (except radioactive promethium) are assigned in Tables 2−13 with the ν_3 (a_1) fundamental also identified for most of these.

LnH_3 Species. The lanthanide trihydride is the second most common nonstoichiometric solid lanthanide hydride[41] and also the second most common molecular reaction product of lanthanide atoms with H_2, appearing in spectra of six out of thirteen systems studied as assigned in the tables. The trihydride (C_{3v}) antisymmetric ν_3 (e) mode is very similar to the antisymmetric ν_3 (b_1) vibration of the dihydride species, and so the trihydride absorption is generally near the dihydride mode, and sometimes coincident. In cases where the trihydride and dihydride coincide, they are differentiated by the HD spectra, where the two species exhibit very different isotopic shifts.

The characteristic hydrogen isotopic shifting pattern of the trihydrides is only a small red shift of the LnH_3 peak upon LnH_2D formation with a concurrent small blue shift of the LnD_3 peak upon formation of $LnHD_2$. These mixed isotopic species also have an infrared-allowed stretch for the odd isotope, which provides an additional peak for the mixed isotopic species. A band present only in high laser power experiments at 1283.1 (918.0) cm^{-1} increases with annealing and is assigned to the ν_3 (e) mode of CeH_3. This band demonstrates the characteristic LnH_3 isotopic shifting pattern in spectra of Ce reacted with HD; the 1283.1 cm^{-1} CeH_3 absorption shifts down 1.5 cm^{-1} to 1281.6 cm^{-1} for the CeH_2D analogue and the 918.0 cm^{-1} CeD_3 absorption shifts up 0.6 cm^{-1} to 918.6 cm^{-1} for the $CeHD_2$ isotopic species.

LnH_4. The antisymmetric stretching modes of the LnH_4 species absorb 150−200 cm^{-1} higher than the respective LnH_2 molecules, and the LnH_4 molecules may have symmetry lower than the anticipated T_d symmetry. For the uranium hydrides, UH_4 is 110 cm^{-1} higher than UH_2,[22] for the hafnium hydrides, HfH_4 is 56 cm^{-1} higher than HfH_2, but not for the ThH_2/ThH_4 pair,[21] where the relativistic contraction of the Th s and p orbitals is canceled by the relativistic expansion of the d and f orbitals in ThH_4,[20] resulting in a separation of only 10 cm^{-1} for the ThH_2 and ThH_4 antisymmetric fundamentals. The LnH_4 spectra, observed here only for CeH_4, NdH_4, SmH_4, and DyH_4, are assigned in the tables.

Symmetric and antisymmetric stretching modes of CeH_4, respectively, are observed at 1500.5 (1070.2) and 1441.8 (1032.1) cm^{-1} (Figure 1). These peaks track together, increasing with annealing up to 25 K and decreasing by half with Hg arc photolysis. In spectra from low laser power experiments, 1441.8 cm^{-1} absorbs weakly, which suggests that this band is due to a reaction product of Ce with molecular, not atomic, hydrogen, and therefore a species containing an even number of H atoms. Spectra of products of atomic Ce reacted with HD yield peaks for the CeH_2D_2 isotopic species at 1493.6 and 1449.4 cm^{-1} for the H stretches, which are presumably uncoupled to the D stretches absorbing at 1065.6 and 1036.2 cm^{-1}. The observation of four distinct Ce−H and Ce−D stretching modes confirms the identification of a tetrahydride molecule. The CeH_4 molecule is expected to be a singlet state, and there is no reason for the 6s 5d 4f valence configuration of Ce to support a tetrahedral molecule. The observed isotopic absorption pattern is appropriate for a CeH_4 molecule of C_{3v} symmetry. The CeH_4 molecule is probably made by reaction of further H_2 with CeH_2 reaction 3.

$$H_2 + CeH_2 \rightarrow CeH_4 \qquad (3)$$

ThH_4, which is demonstrated by relativistic calculations to have a bond length similar to that of CeH_4,[20] has an antisymmetric stretching frequency only 3 cm^{-1} higher than the antisymmetric stretch of CeH_4.[21] In most cases, relativistic contractions of heavy nuclei shorten bond lengths with respect to distances observed for bonds in isoelectronic molecules that contain lighter metals. However, in the case of ThH_4 and CeH_4, the relativistic and shell effects cancel, and the overall difference in bond strengths between the two isoelectronic molecules is therefore small.[20] However, the normal relativistic effects are demonstrated in the ThH_2/CeH_2 pair, for which the ThH_2 antisymmetric fundamental[21] exceeds the CeH_2 antisymmetric fundamental by 170 cm^{-1}.

Three absorptions are attributed to the NdH_4 species (Figure 2): two closely spaced intense antisymmetric modes of NdH_4 are observed at 1300.7 (931.6) cm^{-1} and 1304.3 (935.5) cm^{-1}; the less intense symmetric stretch occurs at 1384.6 (986.3) cm^{-1}. With the $6s^24f^4$ valence configuration for Nd, the NdH_4 molecule is probably a triplet state and subject to Jahn−Teller distortion, presumably to approximately C_{3v} symmetry, but the local symmetry may be lower as the strong antisymmetric mode is split by 3−6 cm^{-1}.

Substitution of HD for H_2 yields only the isotopically substituted NdH_2D_2 analogue (Figure 2), indicating that the formation mechanism of the tetrahydride includes addition of molecular H_2, not atomic H, to the metal center. It is presumed that because of one considerably elongated bond, two distinguishable NdH_2D_2 molecules of C_s symmetry are observed. The species with a long deuterium bond has its most intense absorption, the antisymmetric motion of the two H atoms, at 1301.7 cm^{-1}, and weaker symmetric Nd−H_2 and Nd−D stretches at 1359.4 and 950.6 cm^{-1}. Analogously, the molecule with the long hydrogen bond has its most intense antisymmetric DNdD fundamental at 935.0 cm^{-1}, and symmetric Nd−H and Nb−D_2 stretches at 1331.2 and 1967.0 cm^{-1}. Notice that the antisymmetric stretches of the isotopically substituted molecules fall between the two strong absorptions of the isotopically pure species.

The NdH_4 assignment is 180 cm^{-1} lower than the antisymmetric vibrational frequency of UH_4 because of relativistic contraction of the uranium atomic orbitals, which strengthens the bonding in the isoelectronic UH_4 molecule.[22] This is consistent with the relativistic effects found for the UH_2/NdH_2 pair, for which the UH_2 antisymmetric stretch is 220 cm^{-1} higher than its NdH_2 analogue.[22]

Bridging Hydrogen Species. Hydride stretching modes about 150 cm^{-1} lower than the terminal hydride stretching region are assigned in the tables to bridged hydrogen motions. Bonding to two metal centers weakens the hydride bonds and lowers their stretching frequencies. Because these bands grow on annealing, they are likely due to aggregate species and the smallest such bridged aggregate is the dimer $(LnH)_2$. These stretches are also favored in high laser power experiments, under which condition more monohydride molecules are formed and thus more monohydride dimers.

The absorption observed at 1128.0 (808.3) cm^{-1} is attributed to the stretching motion of the bridging hydrogens in the $(CeH)_2$ molecule (Figure 1). The experiments with HD show four stretches for the CeHCeD molecule at 1195.8, 1125.4, 843.3, and 809.5 cm^{-1}. The higher frequency bands in each region are due to a symmetric motion of H(D), while the two lower frequency bands are due to antisymmetric motions. Spectra in low laser power experiments do not contain bands attributable to $(CeH)_2$ because of lower metal concentration.

Density functional calculations were performed for the $(CeH)_2$ molecule. Optimized geometries were obtained for both puckered C_{2v} and flat D_{2h} molecules with triplet, quintet, and septet multiplicities, and frequencies were calculated for the triplet and quintet states. Energies of the different configurations were indistinguishable within the error of the calculations, but the

frequencies obtained for the D_{2h} triplet state of $(CeH)_2$ most closely resemble the observed fundamental of this molecule. This suggests that the $(CeH)_2$ molecule is planar, or slightly puckered, and that there is double bond character between the cerium atoms. The quintet state provided similar frequencies to the triplet state but calculated one negative frequency, and the septet did not converge in the frequency calculation. Computational results for the D_{2h} triplet state are provided in Table 14.

Higher Order Species. After annealing of argon matrices containing CeH_2 and H_2, bands appear at 1248.6 (894.2) and 1298.8 (927.5) cm^{-1}, with isotopic hydrogen ratios of 1.3963 and 1.4003, respectively. The two bands track together, both decreasing with mercury arc photolysis and increasing with subsequent annealing. In HD experiments, the peaks are replaced by intervening peaks at 1273.3 (910.3) cm^{-1}, characteristic of uncoupled H (D) motions in an isotopically substituted CeH_2 molecule. The less intense, higher absorption has a hydrogen isotopic ratio that indicates a symmetric stretching mode of the CeH_2 unit, while the hydrogen isotopic ratio of the more intense, lower absorption is indicative of an antisymmetric stretch. The increase with annealing is characteristic of complexed species. These bands are assigned to the $(H_2)CeH_2$ complex.

Density functional calculations performed for the H_2 complexed triplet CeH_2 molecule support the assignment of stretching modes of the $(H_2)CeH_2$ complex lower than comparable modes of CeH_2 dihydride (Table 14). The best relative agreement is found for the antisymmetric stretch of the CeH_2 unit, which is calculated to red shift by 46.1 cm^{-1} and experimentally red shifts by 33.1 cm^{-1}. Density functional calculations predict that the symmetric dihydrogen stretching mode should appear near 2880 cm^{-1} with comparable intensity to the antisymmetric CeH_2 stretching mode. However, this band is not observed in the spectrum, presumably because of overestimation of the calculated intensity. Calculated molecular energies predict that reaction 4 is exothermic by 0.25 eV, whereas reaction 3 is

$$H_2 + CeH_2 \rightarrow (H_2)CeH_2 \qquad (4)$$

exothermic by 0.11 eV. The 1248.1 cm^{-1} band in Pr experiments behaves similarly and is likewise assigned to the $(H_2)PrH_2$ complex.

Higher order polymeric gadolinium hydride species show a broad terminal stretch centered at about 1290 (920) cm^{-1} and a broad bridging absorption centered at 1072 (775) cm^{-1}. These broad bands appear on annealing and continue to increase at higher temperatures. Individual molecules of order higher than the dimer cannot be distinguished.

Conclusions

A general study of lanthanide hydride species produced by reaction of laser-ablated metal atoms with molecular hydrogen yields three new monohydride molecules, thirteen new inserted dihydrides, six new trihydrides, four new tetrahydrides, and six new bridged hydride molecules. The most prevalent new species is the molecular lanthanide dihydride that is formed by direct insertion of an ablated metal atom into the H_2 molecular bond. Observation of the HLnD stretching modes at the average of the respective LnH_2 and LnD_2 modes demonstrates the complete decoupling of the H and D vibrations of the HLnD isotopic molecules due to the mass difference between H and D. The uncoupled frequencies observed for HEuD agree with those observed for terminal hydrogen modes in solid-phase EuH_2 and EuD_2, lending general support to the assignments of the lanthanide dihydrides.

In agreement with results obtained from density functional calculations, lanthanide trihydride absorptions were often found to be coincident with dihydride peaks but are differentiated by experiments with isotopic HD. Observations for LnH_4 suggest a lowering of symmetry for CeH_4, NdH_4, and SmH_4, while DyH_4 appears to maintain T_d symmetry in the matrix. More theoretical calculations are suggested to explore this apparent symmetry lowering and to compare with ThH_4 and UH_4 for relativistic effects. Several monohydrides show evidence of dimerization to form bridged hydride species that absorb about 150 cm^{-1} lower than the terminal metal dihydride stretching region.

Acknowledgment. We thank the Air Force Office of Scientific Research for financial support and E. J. Baerends for the ADF code maintained by M. Neurock.

References and Notes

(1) Vajda, P.; Daou, J. N. *Phys. Rev. B (Condens. Matt.)* **1994**, *49*, 3275.
(2) Libowitz, G. G. *Ber. Bunsen-Ges. Phys. Chem.* **1972**, *76*, 837.
(3) Libowitz, G. G.; Pack, J. G. *J. Chem. Phys.* **1969**, *50*, 3557.
(4) McGuiness, P. J.; Zhang, X. J.; Forsyth, H.; Harris, I. R. *J. Less-Common Met.* **1990**, *162*, 379.
(5) Mottram, R. S.; Harris, I. R. *J. Alloys Compounds* **1999**, *283*, 282.
(6) Bauhofer, W.; Joss, W.; Kremer, R. K.; Mattausch, H. J.; Simon, A. *J. Magn, Magn. Mater.* **1992**, *104*, 1243.
(7) Van Zee, R. J.; Seely, M. L.; Weltner, W., Jr. *J. Chem. Phys.* **1977**, *67*, 861.
(8) Kopp, I.; Hagland, L.; Rydh, B. *Can. J. Phys.* **1975**, *53*, 2242.
(9) Sugiyama, K.; Yoda, J. *Phys. Rev. A* **1997**, *55*, R10.
(10) Effantin, C.; D'Incan, J. *Can. J. Phys.* **1973**, *51*, 1394.
(11) D'Incan, J.; Effantin, C.; Bacis, R. *Can. J. Phys.* **1972**, *50*, 1810.
(12) Effantin, C.; D'Incan, J. *Can. J. Phys.* **1974**, *52*, 523.
(13) D'Incan, J.; Effantin, C.; Bacis, R. *Can. J. Phys.* **1977**, *55*, 1654.
(14) D'Incan, J.; Effantin, C.; Bacis, R. *J. Phys. B* **1972**, *5*, L187.
(15) Pyykkö, P. *Phys. Scr.* **1979**, *20*, 647.
(16) Pyykkö, P. *Inorg. Chim. Acta* **1987**, *139*, 243.
(17) Dolg, M.; Stoll, H. *Theor. Chim. Acta* **1989**, *75*, 369.
(18) Dolg, M.; Stoll, H.; Preuss, H. *Chem. Phys.* **1992**, *165*, 21.
(19) Liu, W.; Dolg, M.; Li, L. *J. Chem. Phys.* **1998**, *108*, 2886.
(20) Pyykkö, P.; Desclaux, J. P. *Chem. Phys.* **1978**, *34*, 261.
(21) Souter, P. F.; Kushto, G. P.; Andrews, L.; Neurock, M. *J. Phys. Chem. A* **1997**, *101*, 1287.
(22) Souter, P. F.; Kushto, G. P.; Andrews, L.; Neurock, M. *J. Am. Chem. Soc.* **1997**, *119*, 1682.
(23) Pyykkö, P. *Chem. Rev.* **1988**, *88*, 563.
(24) Chertihin, G. V.; Andrews, L. *J. Am. Chem. Soc.* **1995**, *117*, 6402.
(25) Chertihin, G. V.; Andrews, L. *J. Phys. Chem.* **1995**, *99*, 15004.
(26) Drulis, M. *J. Alloys Compounds* **1993**, *198*, 111.
(27) Burkholder, T. R.; Andrews, L. *J. Chem. Phys.* **1991**, *95*, 8697.
(28) Hassanzadeh, P.; Andrews, L. *J. Phys. Chem.* **1992**, *96*, 9177.
(29) Chertihin, G. V.; Saffel, W.; Yustein, J. T.; Andrews, L.; Neurock, M.; Ricca, A.; Bauschlicher, C. W., Jr. *J. Phys. Chem.* **1996**, *100*, 5261.
(30) Andrews, L.; Bare, W. D.; Chertihin, G. V. *J. Phys. Chem. A* **1997**, *101*, 8417.
(31) Kriegler, R. J.; Welsh, H. L. *Can. J. Phys.* **1968**, *46*, 1181.
(32) Willson, S. P.; Andrews, L. *J. Phys. Chem. A* **1999**, *103*, 3171.
(33) Willson, S. P.; Andrews, L. *J. Phys. Chem. A* **1999**, *103*, 6972.
(34) ADF 2.1. *Theoretical Chemistry*; Vrije Universiteit: Amsterdam.
(35) Baerends, E. J.; Ellis, D. E.; Ros, P. *Chem. Phys.* **1973**, *2*, 41.
(36) teVelde, G.; Baerends, E. J. *Comput. Phys.* **1992**, *99*, 84.
(37) Vosko, S. H.; Wilk, L.; Nusair, M. *Can. J. Phys.* **1980**, *58*, 1200.
(38) Becke, A. D. *Phys. Rev. A* **1988**, *38*, 3098.
(39) Perdew, J. P. *Phys. Rev. B* **1986**, *33*, 8822.
(40) Heinemann, C.; Cornehl, H. H.; Scroder, D.; Dolg, M.; Schwarz, S. *Inorg. Chem.* **1996**, *35*, 2463.
(41) Libowitz, G. G.; Maeland, A. J. *Handb. Phys. Chem. Rare Earths* **1979**, *3*, 299.
(42) Wilson, E. B., Jr.; Decius, J. C.; Cross, P. C. *Molecular Vibrations; the Theory of Infrared and Raman Vibrational Spectra*; McGraw-Hill: New York, 1955.
(43) Field, R. W. *Ber. Bunsen-Ges. Phys. Chem.* **1982**, *86*, 771.
(44) Martin, W. C.; Zalubas, R.; Hagan, L., Eds. *Atomic Energy Levels—The Rare-Earth Elements*; U.S. Department of Commerce, National Bureau of Standards: Washington, DC, 1978.